On the influence of drag force modeling in long-span suspension bridge flutter analysis

AIMETA 2019
XXIV Conference
The Italian Association of Theoretical and Applied Mechanics
Rome, Italy, 15-19 September 2019

ON THE INFLUENCE OF DRAG FORCE MODELING IN LONG-SPAN SUSPENSION BRIDGE FLUTTER ANALYSIS

Gianfranco Piana and Alberto Carpinteri

Politecnico di Torino, Department of Structural, Geotechnical and Building Engineering, Corso Duca degli Abruzzi 24 – 10129 Torino, Italy

E-mail: gianfranco.piana@polito.it, alberto.carpinteri@polito.it

Keywords: aeroelastic flutter, suspension bridge, Akashi Kaikyo Bridge.

Abstract. *The present study aimed at investigating the role played by the description of the drag component on the predicted flutter velocity (and frequency) of very long-span suspension bridges. Based on a detailed finite element model of the central span of the Akashi Kaikyo Bridge, implemented in ANSYS, flutter analyses were run according to the following descriptions of the wind aerodynamic actions: (a) unsteady lift, moment and drag; (b) unsteady lift and moment plus steady drag, and (c) unsteady lift and moment, without drag. The finite element results are compared with those obtained by an* in-house *MATLAB code based on a semi-analytic continuum model. The latter includes flexural-torsional second-order effects induced by steady drag force in the bridge's equations of motion, in addition to the unsteady lift and moment actions.*

1 INTRODUCTION

Flutter stability analysis of long-span bridges is usually conducted as a damped complex eigenvalue analysis, where the aeroelastic (self-excited or motion-dependent) forces acting on the bridge deck are expressed as linear functions of deck's displacements and velocities [1]. In most practical applications, among the general three aeroelastic forces of drag, lift, and pitching moment, only the latter two are of interest, the former being of little importance for dynamic stability. However, it has been shown [2] that, for very long-span bridges like the case of the Akashi Kaikyo Bridge – the current world record for a single span – all the three components must be taken into account to correctly predict the flutter wind velocity.

The present study aimed at investigating the role played by the description of the drag component on the predicted flutter velocity (and frequency) of very long-span suspension bridges. The Akashi Kaikyo Bridge was selected as a benchmark. To the purpose, a detailed finite element model of the central span of the bridge was implemented in ANSYS. The user-defined Matrix27 element [3] was incorporated into the model to define the nodal aeroelastic forces by means of element aerodynamic stiffness and damping matrices. Flutter analyses were thus run considering the following descriptions of the wind aerodynamic actions:

1) Lift, moment and drag all unsteady (motion-dependent);
2) Lift and moment unsteady, drag steady (motion-independent);
3) Lift and moment unsteady, no drag.

The finite element results were compared with those obtained by an in-house MATLAB code based on a semi-analytic continuum model. The latter includes flexural-torsional second-order effects induced by steady drag force in the bridge equations of motion, in addition to the unsteady lift and moment actions.

2 AERODYNAMIC ACTIONS AND FLUTTER ANALYSIS METHODS

2.1 Aerodynamic action modeling

With reference to a deck-girder section model (deck portion of unit length), having at most three degrees of freedom in the plane, linearly damped and elastically supported, the following three descriptions of the aerodynamic actions produced by a laminar transverse wind were adopted in this study:

- Case 1)

$$L_{se} = \frac{1}{2}\rho U^2 B\left(KH_1^* \frac{\dot{h}}{U} + KH_2^* \frac{B\dot{\alpha}}{U} + K^2 H_3^* \alpha + K^2 H_4^* \frac{h}{B} + KH_5^* \frac{\dot{p}}{U} + K^2 H_6^* \frac{p}{B} \right), \tag{1}$$

$$D_{se} = \frac{1}{2}\rho U^2 B\left(KP_1^* \frac{\dot{p}}{U} + KP_2^* \frac{B\dot{\alpha}}{U} + K^2 P_3^* \alpha + K^2 P_4^* \frac{p}{B} + KP_5^* \frac{\dot{h}}{U} + K^2 P_6^* \frac{h}{B} \right), \tag{2}$$

$$M_{se} = \frac{1}{2}\rho U^2 B^2\left(KA_1^* \frac{\dot{h}}{U} + KA_2^* \frac{B\dot{\alpha}}{U} + K^2 A_3^* \alpha + K^2 A_4^* \frac{h}{B} + KA_5^* \frac{\dot{p}}{U} + K^2 A_6^* \frac{p}{B} \right), \tag{3}$$

where: L_{se}, D_{se}, M_{se} are the unsteady (self-excited) aerodynamic actions of lift, drag, and moment per unit length, respectively; ρ is the air mass density; U is the wind speed; B is the deck width; $K = \omega B/U$ is the reduced circular frequency (ω is the circular frequency); h, p, α

are the vertical (heaving), lateral (sway), torsional generalized displacements, respectively (dotted symbols represent time derivatives); H_i^*, P_i^*, A_i^* are the non-dimensional flutter derivatives, which are functions of *K*. They are usually evaluated in the wind tunnel for the deck section of interest, and plotted as functions of the reduced velocity $U_r = 2\pi / K$ [4,5].

- Case 2)

Lift and moment were assumed as self-excited forces according to Eqs. (1) and (3), respectively, while the drag force was assumed as a steady force as follows:

$$D_s(0) = \frac{1}{2}\rho U^2 B\, C_D(0), \tag{4}$$

where $C_D(0)$ is the steady drag coefficient, which is a function of the deck section and wind attack angle, evaluated for zero angle of attack [4,5].

- Case 3)

Lift and moment were assumed as self-excited forces according to Eqs. (1) and (3) as in the previous cases, while the drag force was discarded.

2.2 Finite element flutter analysis

The finite element setting for linear flutter analysis writes as follows:

$$\mathbf{M}\ddot{\mathbf{X}} + \left(\mathbf{C} - \mathbf{C}^*\right)\dot{\mathbf{X}} + \left(\mathbf{K} - \mathbf{K}^*\right)\mathbf{X} = \mathbf{0}, \tag{5}$$

where: $\mathbf{M}, \mathbf{C}, \mathbf{K}$ are the global mass, damping, and stiffness matrices, $\mathbf{C}^*, \mathbf{K}^*$ are the aerodynamic damping and stiffness matrices, respectively, all obtained by assembly of the corresponding local (element) matrices; $\mathbf{X}$ is the dynamic response vector. $\mathbf{C}^*, \mathbf{K}^*$ are evaluated based on the aerodynamic loading descriptions in Section 2.1, adopting a lamped formulation.

By Eq. (5), a damped complex eigenvalue analysis can be carried out to study dynamic stability of the discretized bridge structure for increasing wind speeds. The dynamic response can be approximated by a superposition of the first *m* conjugate pairs of complex eigenvalues and eigenvectors, as:

$$\mathbf{X} = \sum_{j=1}^{m} \mathbf{x}_j \, \mathrm{e}^{\lambda_j t}, \tag{6}$$

where $\mathbf{x}_j = \mathbf{p}_j \pm \mathrm{i}\mathbf{q}_j$ is the j^{th} complex conjugate pair of eigenvectors, $\lambda_j = \sigma_j \pm \mathrm{i}\omega_j$ is the j^{th} complex eigenvalue.

The system is dynamically stable if the real part of all eigenvalues is negative and dynamically unstable if the real part of one or more eigenvalues is positive. The condition for occurrence of flutter instability is then identified as follows: for certain wind velocity U_f the system has one complex eigenvalue λ_f with zero or near zero real part, the corresponding wind velocity U_f being the critical flutter wind velocity and the imaginary part of the complex eigenvalue λ_f

becoming the flutter frequency. A mode-by-mode tracing method must be employed to iteratively search for the flutter frequency and determine the critical flutter wind velocity.

2.3 Semi-analytic continuum model for flutter analysis with drag-induced second-order effects

With reference to the single-span suspension bridge scheme, the structure is composed by a deck-girder, modeled as an elastic beam of constant cross-section, deformable in flexure and torsion, while inextensible and not deformable in shear, vertically suspended to the main cables, modeled as tension-only elastic elements, by a continuous system of hangers, modeled as inextensible bars. The deck-girder is simply supported at the ends for both bending and torsion, and is supposed to be straight under permanent loads. The pair of main suspending cables, having shallow parabolic profile, is connected to fixed points with same height. A fictitious elastic modulus of the cables is introduced to suitably take into account the compliance of the end portions of the cables between towers and anchorages.

According to the previous assumptions, under the action of uniformly distributed steady drag force and unsteady lift and moment, the equations of motion of the deck-girder, described in terms of vertical deflection, $v(z,t)$, and torsion rotation of the beam sections, $\vartheta(z,t)$, where *z* is the abscissa measured along the beam centroidal axis and *t* is time, write:

$$\mu_g \ddot{v} + c_v \dot{v} + EI_x v'''' - Hv'' + \left(m_y \vartheta\right)'' - y_c''\left(h_R(t) + h_L(t)\right) = L_{se}, \tag{7}$$

$$I_\vartheta \ddot{\vartheta} + c_\vartheta \dot{\vartheta} + EI_\omega \vartheta'''' - \left(GI_t + Hb^2\right)\vartheta'' + m_y v'' + b\, y_c''\left(h_R(t) - h_L(t)\right) = M_{se}, \tag{8}$$

where: μ_g, I_ϑ are the bridge's (deck-girder, cables and hangers) mass, polar mass moment of inertia per unit length; $c_v = 2\mu_g \zeta_v \omega_v$, $c_\vartheta = 2I_\vartheta \zeta_\vartheta \omega_\vartheta$ are the damping coefficients (with ζ_v, ζ_ϑ the damping ratios, $\omega_v, \omega_\vartheta$ the angural frequencies); EI_x is the bending rigidity in the vertical plane (*x* is the cross-section horizontal axis through the centroid); EI_ω, GI_t are the warping (Vlasov), primary (St. Venant) torsion rigidities; H is the total horizontal component of the main cables tension due to the bridge weigth per unit length, q_g ($H = q_g l^2 / 8f$, with *l* the bridge (central) span and f the cables sag); $m_y = D_s(0)\, z\, (l - z)/2$ is the bending moment in the horizontal plane, due to the steady drag, $D_s(0)$, given by Eq. (4) (*y* is the cross-section vertical axis through the centroid); y_c is the initial profile of the main cables, assumed parabolic. Overdots denote differentiation with respect to time *t*, apexex denote differentiation with respect to *z*. h_R, h_L are the additional horizontal components of the rigth, left cable tensions (nil for antisymmetric deformations), given by:

$$h_R(t) = \frac{E_c\left(A_c/2\right)}{l}\frac{q_g}{H}\int_0^l \left(v(z,t) - b\,\vartheta(z,t)\right)\mathrm{d}z, \qquad h_L(t) = \frac{E_c\left(A_c/2\right)}{l}\frac{q_g}{H}\int_0^l \left(v(z,t) + b\,\vartheta(z,t)\right)\mathrm{d}z,$$

where E_c is the Young's modulus and A_c is the total cross-sectional area of the main cables, *b* is the half-width between the main cables.

The self-excited actions of lift and moment, L_{se} and M_{se}, are expressed as follows:

$$L_{se} = \frac{1}{2}\rho U^2 B\left(KH_1^*(K)\frac{\dot{v}}{U} + KH_2^*(K)\frac{B\dot{\vartheta}}{U} + K^2 H_3^*(K)\vartheta + K^2 H_4^*(K)\frac{v}{B}\right), \tag{9}$$

$$M_{se} = \frac{1}{2}\rho U^2 B^2\left(KA_1^*(K)\frac{\dot{v}}{U} + KA_2^*(K)\frac{B\dot{\vartheta}}{U} + K^2 A_3^*(K)\vartheta + K^2 A_4^*(K)\frac{v}{B}\right), \tag{10}$$

with the same meaning of symbols already introduced in Section 2.1.

Note that Eqs. (7) and (8) are coupled because of the presence of the bending moment m_y induced by the drag force, which produces the destabilizing second-order effects $(m_y\vartheta)''$ and $m_y v''$ [6]. The dynamic solution to Eqs. (7,8) is sought in the form:

$$v(z,t) = \sum_{j=1}^{m} \eta_j(z)\, \mathrm{e}^{\mathrm{i}\omega_j t}, \qquad \vartheta(z,t) = \sum_{j=1}^{m} \psi_j(z)\, \mathrm{e}^{\mathrm{i}\omega_j t}, \tag{11a, b}$$

where the eigenfunctions $\eta_j(z)$ and $\psi_j(z)$ are expressed as series of sine functions [7], and $\omega_j = \omega_{r,j} + \mathrm{i}\,\omega_{i,j}$ is the j^{th} complex eigenvalue. In this case, dynamic instability (i.e. flutter) occurs when the imaginary part of one or more eigenvalues becomes negative, the corresponding real part becoming the flutter frequency ω_f.

Antisymmetric and symmetric modes are analysed separately: the former are expressed as a series of sine functions with even number of half-waves (2, 4, 6, …), while the latter by a series of sine functions with odd number of half-waves (1, 3, 5, …). Eventually, the following complex eigenvalue problem (of dimension 2×2) is obtained:

$$\det\left[-\omega^2\mathbf{M} + \mathrm{i}\omega\left(\mathbf{C} - \mathbf{C}^*\right) + \left(\mathbf{K} - \mathbf{K}_g^D - \mathbf{K}^*\right)\right] = 0, \tag{12}$$

where $\mathbf{K}_g^D$ is the geometric stiffness matrix associated to the drag-induced second-order effects, i.e. the initial stress matrix due to $D(0)$, the remaining symbols having the same meaning already introduced. From Eq. (12), ω^2 values are obtained as functions of (U, U_r). Also in this case, a mode-by-mode tracing method must be employed to iteratively look for the critical (flutter) couple (U_{rf}, ω_f). The flutter wind velocity is thus obtained as $U_f = \omega_f B U_{rf} / 2\pi$.

3 CASE STUDY AND RESULTS

Fig. 1 show the general layout of the Akashi Kaikyo Bridge, while the main geometrical and mechanical properties are listed in Tab. 1.

Property	Measure	Property	Measure
Central span length (m)	1,991	Diameter of hangers (m)	0.19
Side spans length (m)	960	Inertia moment for vertical bending (m^4)	24
Towers height (m)	282.6	Inertia moment for lateral bending (m^4)	130
Truss girder width (m)	35.5	Inertia moment for torsion (m^4)	17.8
Truss girder depth (m)	14	Deck-girder mass (t/m)	28.7
Diameter of main cables (m)	1.12	Polar inertia moment of girder (tm^2/m)	5,800

Table 1: Main geometrical and mechanical properties of the Akashi Kaikyo Bridge.

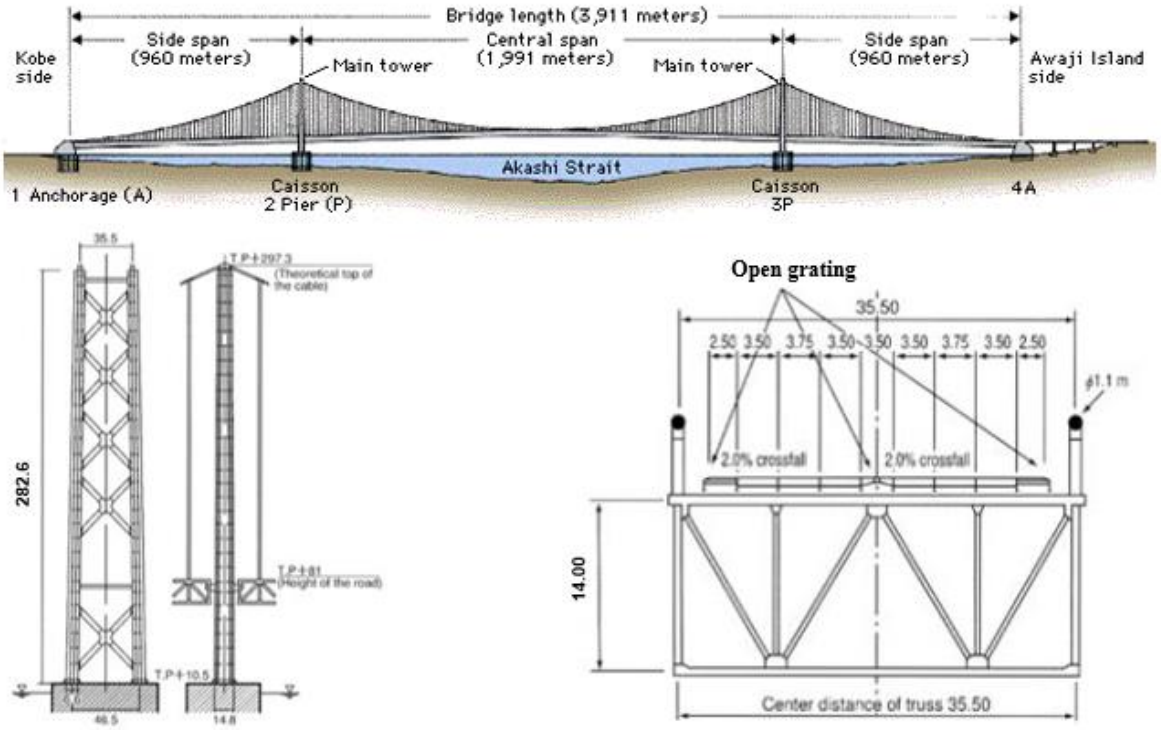

Figure 1: Geometric layout of the Akashi Kaikyo Bridge.

A finite element model of the central span was implemented in ANSYS 15.0 (Fig. 2). BEAM188 finite element was adopted to model main cables and truss girder, whereas LINK180 element was assigned to hangers. A modal analysis without wind action was run in the pre-stressed condition under permanent loads prior to flutter analysis. The flutter derivatives of interest, necessary to define the aerodynamic stiffness and damping matrices through the Matrix27 element, were taken from Katsuchi et al. [8].

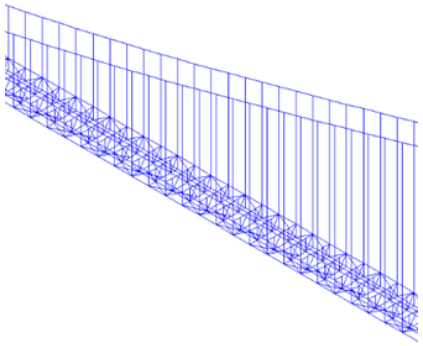

Figure 2: FEM model of the central span implemented in ANSYS 15.0.

Fig. 3 shows the results of flutter analysis in Cases 1, 2 and 3. Real and imaginary parts of complex eigenvalues λ are shown in the left and right panels, respectively. The first symmetric (S) and antisymmetric (A) torsional (T) and vertical (V) eigenvalues are plotter against the mean wind speed U. Flutter velocity and frequency are respectively equal to 81.3 m/s and 0.122 Hz in Case 1 (Fig. 3a), 76.4 m/s and 0.131 Hz in Case 2 (Fig. 3b), whereas no flutter was detected within the 0–100 m/s wind speed range in Case 3 (Fig. 3c).

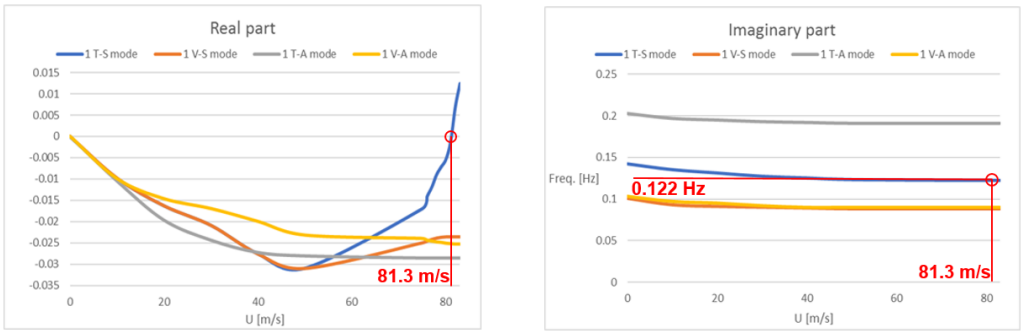

(a)

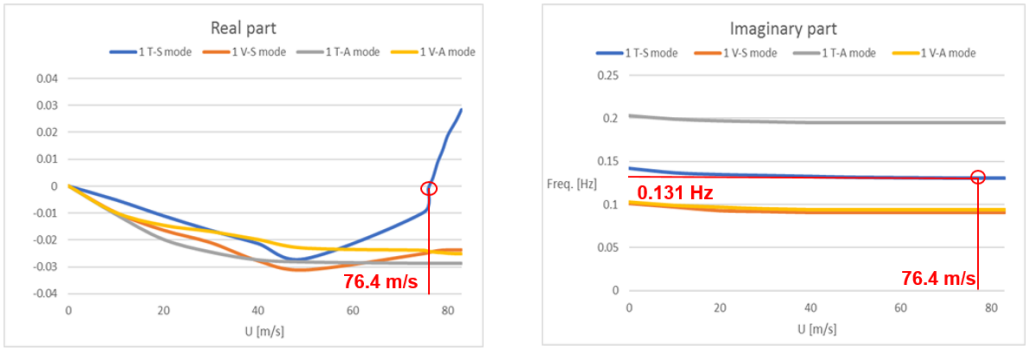

(b)

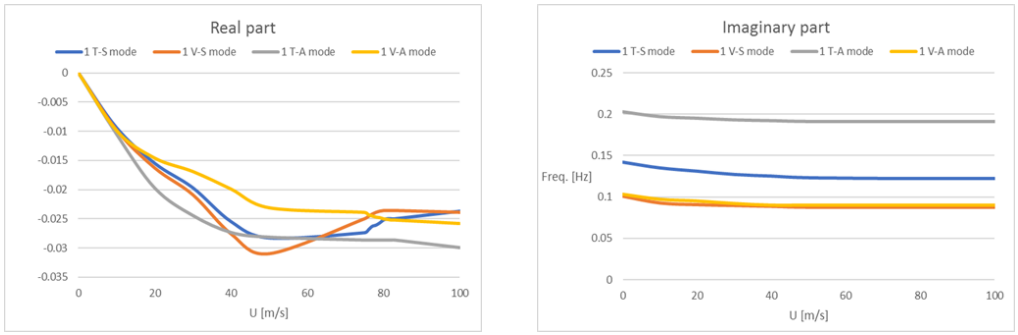

(c)

Figure 3: Real and imaginary parts of complex eigenvalues λ from FEM flutter analysis in Case (a) 1, (b) 2 and (c) 3.

Property	Measure	Property	Measure
l (m)	1,991	I_θ (kgm^2/m)	9.83E+06
f (m)	219	q_g (kg/m)	429,580
E (N/m^2)	2.10E+11	E_c (N/m^2)	1.60E+10
G (N/m^2)	8.08E+10	A_c (m^2)	1.976
B (m)	35.5	b (m)	17.75
I_x (m^4)	24	ρ (kg/m^3)	1.25
I_ω (m^6)	0	$C_D(0)$ (/)	0.421
I_t (m^4)	17.8	ζ_v (%)	0.5
μ_g (kg/m)	43,790	ζ_g (%)	0.3

Table 2: Input parameters adopted for the continuum reduced model of the Akashi Kaikyo Bridge.

Tab. 2 lists the input parameters adopted for the continuum reduced model of the Akashi Kaikyo Bridge. As in the previous case, flutter derivatives of interest were taken from Katsuchi et al. [8]. The numerical solution to Eq. (12) was obtained in MATLAB.

Fig. 4 shows the solution to the flutter problem obtained by the semi-analytic continuum model. The critical condition is identified by U_{rf} = 28.354 and ω_f = 0.469 rad/s, corresponding to a flutter wind velocity U_f = 75.6 m/s and a flutter frequency of 0.075 Hz. The mode responsible for flutter instability is the first of symmetrical torsion.

Tab. 3 collects the results in terms of flutter speed and frequency obtained from both FEM and continuum model analysis. In the same table, experimental values from literature ([2]) are reported as reference; percentage differences between present study and experimental results are indicated by Δ.

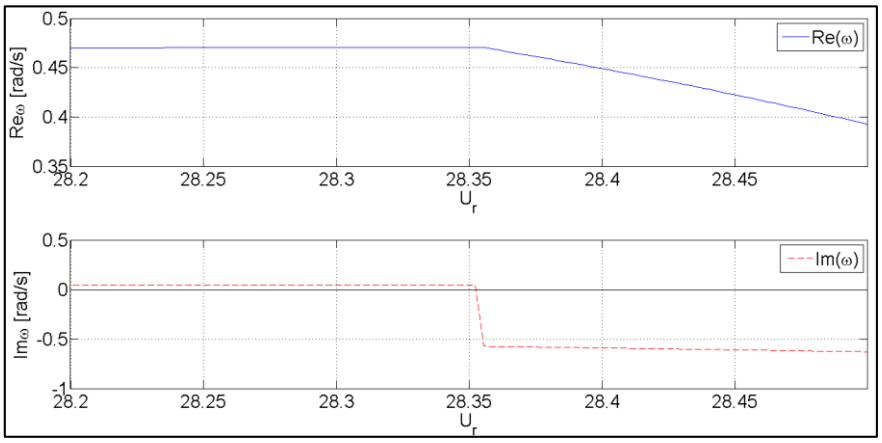

Figure 4: Real and imaginary part of critical complex eigenvalue ω from continuum model.

Flutter param.	Exp. value (from [2])	FEM (L_{se}+M_{se}+D_{se})	FEM (L_{se}+M_{se}+D_s)	FEM (L_{se}+M_{se})	Continuum model (L_{se}+M_{se}+D_s)
U_f (m/s)	84.0	81.3 (Δ = –3.2 %)	76.4 (Δ = –9.0%)	-	75.6 (Δ = –10.0%)
ω_f (Hz)	0.135	0.122 (Δ = –9.6%)	0.131 (Δ = –3.0%)	-	0.075 (Δ = –44.4%)

Table 3: Comparison of FEM, continuum model and experimental results for flutter speed and frequency.

4 FINAL REMARKS AND CONCLUSIONS

In this contribution, we investigated the influence of the drag force component on the predicted flutter velocity, and frequency, of the Akashi Kaikyo Bridge by finite element analysis and a semi-analytic continuum model. A detailed finite element model of the central span was implemented in ANSYS, and flutter analyses were run according to the following description of the aerodynamic loads: (1) unsteady lift, moment and drag; (2) unsteady lift and moment, plus steady drag; and (3) unsteady lift and moment, without drag. The unsteady (motion-dependent) forces were described by means of the user-defined Matrix27 element [3], in terms of aerodynamic stiffness and damping matrices based on the bridge's flutter derivatives available in the literature. Flutter was also analyzed by an *in-house* MATLAB code based on a semi-analytic continuum model of the bridge's central span; the latter includes flexural-torsional second-order effects induced by steady drag force in the equations of motion, plus the unsteady lift and moment actions. For both the FEM and semi-analytic approaches, dynamic stability was analyzed by a classic complex eigenvalue analysis.

For the analyzed case, with respect to literature results, the analyses indicate that including the drag force is, in facts, necessary to correctly estimate the flutter velocity, but also indicate that good predictions can be obtained by combining steady drag together with unsteady lift and moment, if geometric nonlinearity in the deck is taken into account.

REFERENCES

[1] R.H. Scanlan, Developments in aeroelasticity for the design of long-span bridges. T. Miyata et al. eds., Long-Span Bridges and Aerodynamics. *Proceedings of the International Seminar Bridge Aerodynamics Perspective*, Kobe, March 1998, Springer, Tokyo, 1999.

[2] T. Miyata et al., New findings of coupled-flutter in full model wind tunnel tests on the Akashi Kaikyo Br. *Proceedings of the International Conference on Cable-Stayed and Suspension Bridges*, Vol. 2, Deauville, France, 1994.

[3] X.G. Hua et al., Flutter analysis of long-span bridges using ANSYS. *Wind and Structures*, **10**(1), 61-82, 2007.

[4] E. Simiu, D. Yeo, *Wind Effects on Structures: Modern Structural Design for Wind, 4th Edition*. Wiley, 2019.

[5] J.A. Jurado et al., *Bridge Aeroelasticity: Sensitivity Analysis and Optimal Design*. WIT Press, 2011.

[6] G. Piana et al., Natural Frequencies of Long-Span Suspension Bridges Subjected to Aerodynamic Loads, *Dynamics of Civil Structures, Volume 4: Proceedings of the 32nd IMAC*, Springer, 2014.

[7] F. Bleich et al., *The mathematical theory of vibration in suspension bridges: A contribution to the work of the Advisory Board on the Investigation of Suspension Bridges*. University of Michigan Library, 1950.

[8] H. Katsuchi et al., Multi-mode flutter and buffeting analysis of the Akashi-Kaikyo bridge. *Journal of Wind Engineering and Industrial Aerodynamics*, **77-78**(1), 431-441, 1998.